Chapter 4

Giant Magnetoresistance in Organic Spin Valves

4.1 Introduction

Advances in nanoscale science are paving the way towards an entire new family of devices. It is now possible to envision systems where a single molecule comprising only a handful of atoms can perform the same type of task that is at present performed by significantly larger solid-state devices. We are now faced with endless possibilities.

As described before, the seminal work by Reed *et al.* [4] has shown one possible way to produce devices based on organic-molecule technology. Since then, other publications in the field have delivered a series of exciting results [4, 25, 26, 203] that show a wide range of phenomena ranging from switching and memory [25, 204] to rectification [205]. Some of these recent developments present real potential for applications.

The use of organic molecules for electronics has recently found its way into the field of magnetotransport [88]. The use of the spin degree of freedom opens new and interesting possibilities. In this area, the spin valve is the model device: two magnetic materials sandwiching a non-magnetic one. The mechanism determining the spin-transport properties derives from the interplay between the orientation of the electrodes' magnetic moments and the coupling of the different spin components to the spacer.

Recent work by Petta *et al.* [49] and Xiong *et al.* [50] has both shown magnetoresistance effects in organic molecules sandwiched between magnetic current/voltage electrodes. In the former, the authors have studied spin transport through organic tunnelling junctions formed by layering octane-dithiolate between nickel leads, whereas in the latter, aromatic molecules were intercalated in between cobalt and $LaMnO_4$.

In both cases the authors have shown that magnetoresistance is possible although perfect reproducibility of the results is still absent. In the case of Petta and coworkers the authors found a maximum GMR ratio of approximately 18 % , with a large sample to sample variation of MR which also included negative values.

In this chapter *Smeagol* is used to throughly study magneto-transport in molecular spin valves. We have considered two different families of molecules that present distinct transport mechanisms, namely coherent tunnelling and ballistic conductance. We give a detailed account of the states participating in the conductance. We also present the underlying effects driving the magnetoresistance and propose a way of engineering new devices using different anchoring groups between molecules and electrodes. Finally we use the idea of asymmetry-induced charging effects to simulate spin polarised STM-like experiments where an organic molecule is adsorbed on a surface and is probed by an STM tip, both of which magnetic.

In the following sections we present our *ab initio* transport calculations using the typical spin valve configuration. We consider two possible alignments of the leads' magnetisation: antiparallel (AA) or parallel (PA). Figure (4.1) shows a ball and stick sketch of one such molecule (1,4-benzene-dithiolate in this case) with the arrows pointing in the direction of the local magnetisation. The sulphur atom is used as the standard anchoring group due to strong bonding to gold [179, 180] and, in our case, nickel [206].

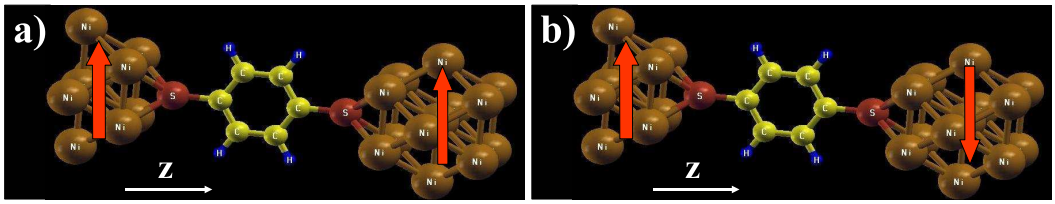

Figure 4.1: 1,4-benzene dithiolate (one benzene ring functionalised by two sulphur atoms at positions 1 and 4) attached via sulphur atoms to two [001]-oriented nickel electrodes. The orientation of the magnetic moments can be either a) parallel or b) anti-parallel.

Going to the details of our calculations, we always construct the unit cell of the extended molecule including four nickel atomic planes on each side. We use standard scalar relativistic pseudopotentials with the following reference configurations: H $1s^1 2p^0$, C $2s^2 2p^2 3d^0$, S $3s^2 3p^4 3d^0$ and Ni $4s^1 4p^0 3d^9$. Furthermore, for good convergence we need to consider a rather rich basis set. For both the molecules we have used a single zeta basis for H, C and S s orbitals, double zeta for Ni s, p and d, and double zeta polarised for C and S p orbitals [40]. This basis gives us a Hamiltonian

with over a thousand degrees of freedom. The LSDA exchange-correlation functional is used throughout. Finally the charge density is obtained by integrating the non-equilibrium Green function over 50 imaginary and 600 real energy points according to the scheme described in chapter (1) and references [70, 71].

4.2 Triphenyl-dithiolate: metallic regime

First we consider 1,4-[3]-phenyl-dithiolate (tricene) consisting of three benzene rings functionalised by thiol groups at both ends. A description of the molecule is presented in figure (4.2a). The molecule is attached to a Ni [001] surface terminated with a pyramid of nickel atoms. The molecule is connected to the hollow site of the nickel surface by the thiolate group. Although a multitude of other anchoring situations may be present in actual samples, this seems to be the most stable for the thiolate group on [001] Ni [206]. We always relax the atomic coordinates of the molecule on the surface using a conjugate gradient method within DFT [40] with a tolerance on the forces of 0.01 eVÅ^{-1}. The relaxations were performed taking a single surface of nickel and attaching the molecule via S-Ni bonds. These were then allowed to relax in a super cell with no periodic boundary conditions. The final relaxed distance between the Ni surface and the S atom was found to be 1.26 Å. We then attached the other surface to the remaining sulphur atom to form the actual junction.

Before calculating the transport properties of this system it is interesting to understand the electronic configuration of the isolated molecule. The density of states and the charge-density iso-surfaces of the highest occupied and lowest unoccupied molecular orbital (HOMO and LUMO) for the isolated molecule are presented in Fig (4.2b). We can see that the HOMO-LUMO gap is approximately 2.5 eV. Moreover the HOMO and LUMO states of tricene are delocalised throughout the whole molecule with charge density concentrated both on the end-groups and on the central phenyl groups. We can clearly see from the iso-surface plots that all the states closes to E_F consist of delocalised π orbitals (carbon $2p_z$ and sulphur $3p_z$ states). However the symmetry of these states is notably different as one can see from the position of the nodes and crests in the local charge density plots.

Figure (4.3) shows the current and zero-bias transmission coefficients for triphenyl-dithiolate. We can see that the transport is through extended states delocalised over the entire molecule and the typical transmission coefficients approach unity. The low-bias resistance of such a device is therefore in the 10 kΩ range. In the parallel case the zero-bias conductance is dominated at the Fermi level by majority spins,

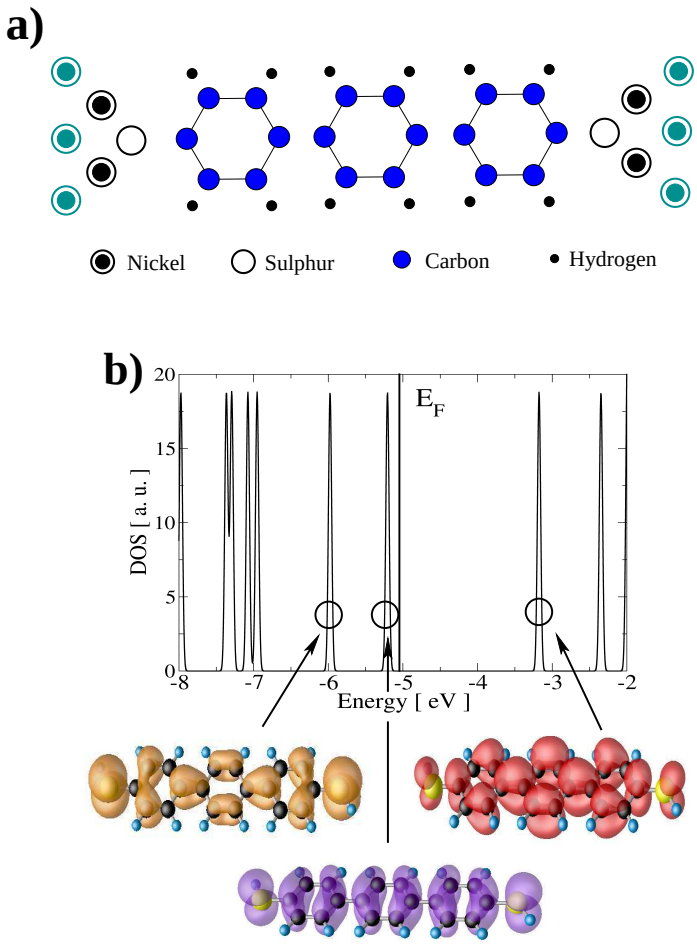

Figure 4.2: Structural and electronic properties of a Ni[001]/tricene/Ni[001] spin-valve. a) Schematic structure of the molecule attached to [001] Ni surfaces. b) Density of states and charge-density iso-surface plots for the relevant molecular orbitals of the isolated tricene-dithiol molecule. The highest "circled" state is the LUMO while the state closest to the Fermi level is the HOMO. A third state is also highlighted (shown in yellow). Because isolated levels correspond to delta functions in the DOS, for display purposes and to aid comparison with Figs (4.3) and (4.5) we have artificially broadened the DOS by 0.1 eV.

with negligible contribution from the minority electrons. The minority spin conduction starts at about 0.1 eV above E_F and is dominant for energies up to 0.6 eV. At higher energies the transmission coefficients become spin-independent because only the unpolarised s electrons are available in the leads. In the antiparallel case there is a general suppression of the transmission coefficients at any energy. For energies

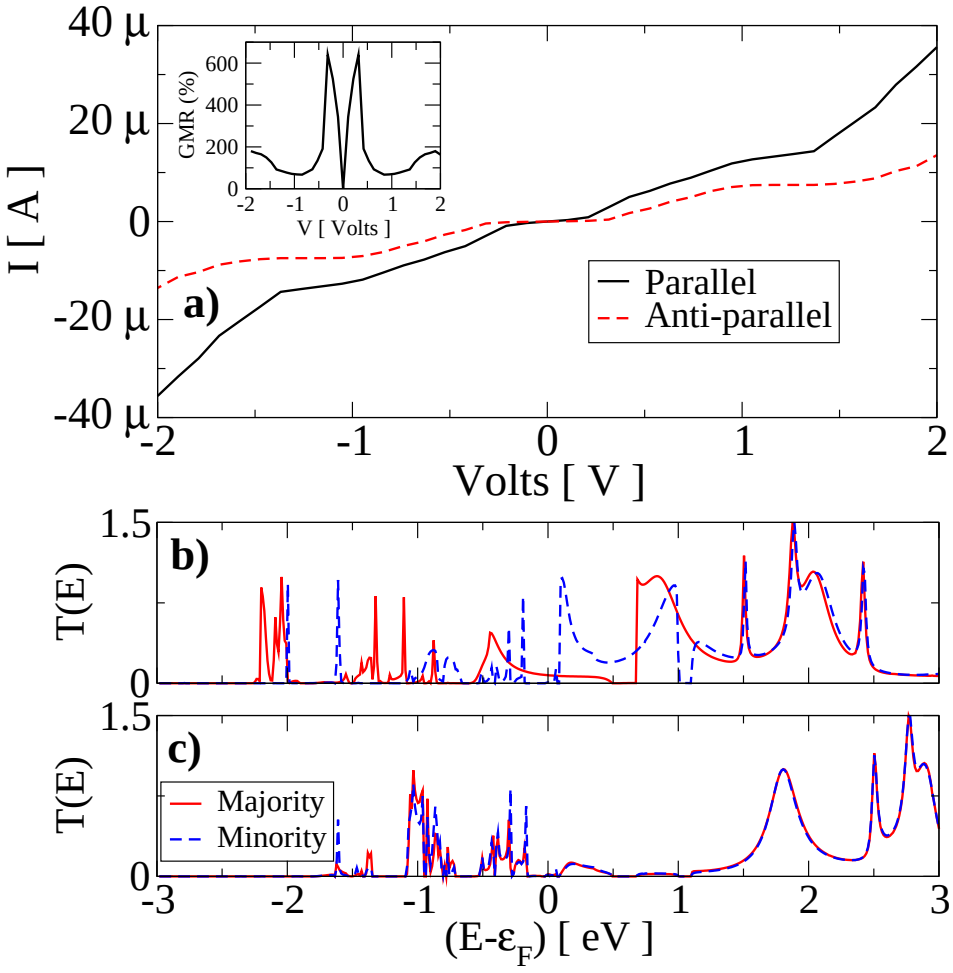

Figure 4.3: a) I-V characteristics for tricene. b) Transmission coefficients at zero bias for majority (solid) and minority (dashed) spins. The inset shows the magnetoresistance as a function of bias.

close to the Fermi level, this appears as a convolution of the transmission in the majority and minority spins in the parallel case. The conductance at the Fermi level is therefore small, and the current shows a tiny zero conductance plateau around zero bias with a consequent very large magnetoresistance ratio, exceeding 600 % close to zero-bias.

We have made additional calculations for various 1,4-[n]-phenyl-dithiolate molecules with different n (n = 1, 2, 3, 4). These curves are presented in figure (4.4) for the PA configuration. We can see that, in general, the features of the zero-bias transmission coefficients are similar and not strongly dependent on the length of the molecule. There is a reduction of the transmission with length, although the decay is certainly

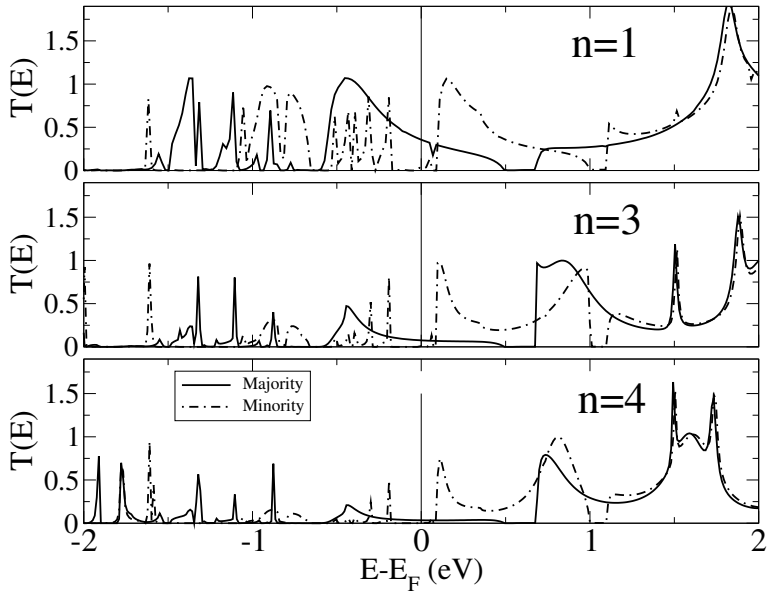

Figure 4.4: Transmission coefficient as a function of energy for 1,4-[n]-phenyl-dithiolate molecules with n=1, 3, and 4. Here the spin-valve is in the parallel configuration. A similar scaling of the transmission coefficient as a function of n is found for the antiparallel configuration.

not exponential, and most importantly the high transmission peaks around the Fermi level remain. Therefore in this class of molecules the transport seems to be appropriately described by a coherent resonant tunnelling mechanism through extended molecular states.

In general one would expect the conductance to be dominated by resonant transport either through the HOMO or the LUMO state of the molecule [178]. This results in peaks in the zero bias transmission coefficient as a function of energy, and usually one is able to identify those corresponding to the HOMO and LUMO gap. In the case of 1,4-phenyl-dithiolate with gold electrodes, the HOMO-LUMO peaks are clearly visible and well separated [178]. In contrast, for the 1,4-tricene-dithiolate with nickel studied here the situation seems different. In fact the transmission coefficients for the parallel case show two peaks respectively for majority and minority spins with a separation of only 0.5 eV, not corresponding to the HOMO-LUMO gap. To identify these states we have followed the evolution of the orbital-resolved density of states (DOS) for a tricene molecule attached to nickel as a function of the Ni-S separation. In particular we have investigated the dependence of the carbon $2p$ and sulphur $3p$ DOS, because these are the relevant orbitals for the bonding to the nickel surface. This is presented in Fig. (4.5). From the figure one notices that the two sulphur p

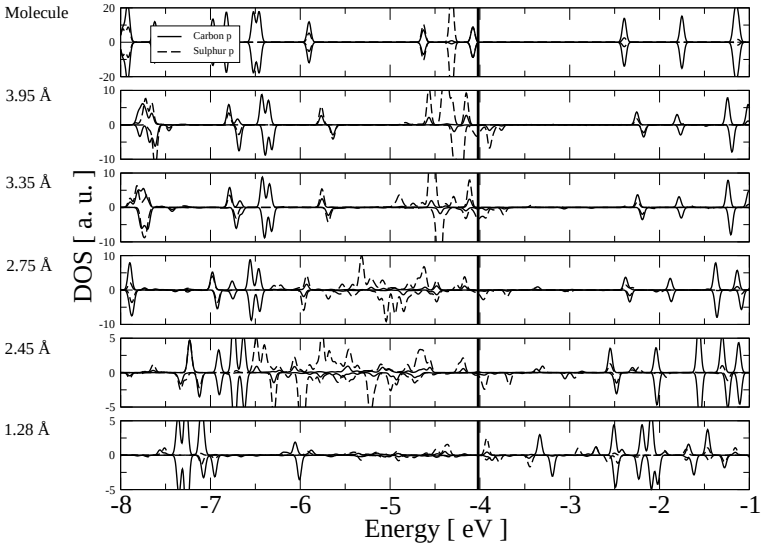

Figure 4.5: Orbital resolved density of states for tricene as a function of the distance between the sulphur end group and the plane of Ni atoms forming the leads. The solid (dashed) line represents the p orbital of carbon (sulphur).

HOMO states of the isolated tricene molecule steadily spin-split and broaden as the Ni-S distance is decreased. At the equilibrium position (1.28 Å) the broadening is large, although at the Fermi level one can still identify two sulphur p states for the majority spin (-0.5 eV and 0.1 eV from E_F) and one for the minority (0.1 eV from E_F). We can then conclude that the transport is through a very broadened HOMO which also includes some contribution from the state 1 eV below the HOMO (shown as a yellow surface in Fig. (4.2)). Also, in tricene molecules, the sulphur atoms posses a tiny spin-polarisation, which is a further indication of strong coupling ($\sim 0.05\mu_B$).

An interesting feature is that, in first approximation, the transmission coefficient at zero bias for the antiparallel state appears to be a convolution of those for the majority and minority spin in the parallel case. This finding can be qualitatively understood in terms of transport through a single molecular state (see figure 4.6). Let $t^{\uparrow}(E)$ be the majority spin hopping integral from one of the leads to the molecular state, and $t^{\downarrow}(E)$ the same quantity for the minority spins. Then, neglecting multiple scattering (i.e. all interference effects), the total transmission coefficients of the entire spin-valve in the parallel state can be written as

$$T^{\uparrow\uparrow}(E) = (t^{\uparrow})^2 \quad \text{and} \quad T^{\downarrow\downarrow}(E) = (t^{\downarrow})^2, \tag{4.1}$$

respectively for the majority and minority spins. The total spin in the parallel

configuration is then

$$T^{\mathrm{PA}}_{\mathrm{Total}} = T^{\uparrow\uparrow} + T^{\downarrow\downarrow}. \tag{4.2}$$

Similarly the transmission in the anti-parallel configuration is

$$T^{\uparrow\downarrow}(E) = T^{\downarrow\uparrow}(E) = t^{\uparrow}t^{\downarrow}, \tag{4.3}$$

$$T^{\mathrm{AA}}_{\mathrm{Total}} = 2T^{\downarrow\uparrow}. \tag{4.4}$$

Thus $T^{\uparrow\downarrow}(E)$ is a convolution of the transmission coefficients for the parallel case

$$T^{\mathrm{AA}}_{\mathrm{Total}} = 2T^{\uparrow\downarrow} \propto 2\sqrt{T^{\uparrow\uparrow}T^{\downarrow\downarrow}}. \tag{4.5}$$

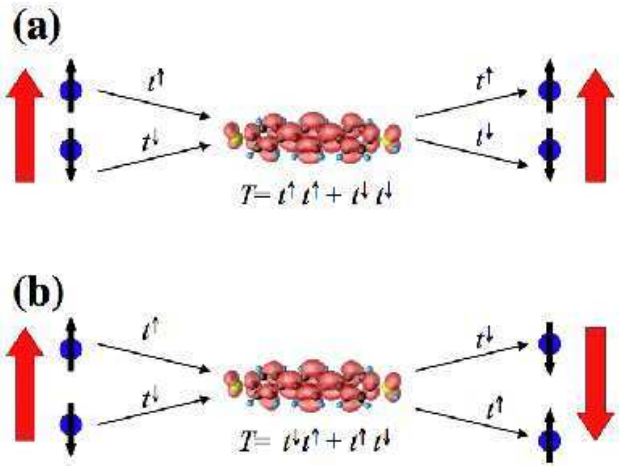

Figure 4.6: Scheme of the spin-transport mechanism through a single molecular state. $t^{\uparrow}(E)$ ($t^{\downarrow}(E)$) is the majority (minority) spin hopping integral from one of the leads to the molecular state. Neglecting quantum interference, in the parallel case (a) the total transmission coefficient is simply $T = (t^{\uparrow})^2 + (t^{\downarrow})^2$, while in the antiparallel (b) $T = 2t^{\uparrow}t^{\downarrow}$. Note that if either $t^{\uparrow}$ or $t^{\downarrow}$ vanishes, the current in the antiparallel configuration will also vanish (infinite GMR).

To further corroborate this picture we can turn our attention to the local charge density between energies E_{min} and E_{max},

$$\Delta n\left(\vec{r}\right) = \sum_{l}^{E_{min}\leq E\leq E_{max}} \left|\Psi_l\left(\vec{r}\right)\right|^2. \tag{4.6}$$

Let us first analyse the PA configuration. Figure (4.7Aa-b) shows the local charge density iso-surfaces for both minority and majority for single particle states with energies comprised in $[-0.5, 0.0]$ eV. We can see that for majority spins there is

charge centred on the carbon atoms along the entire molecule whereas for minority spins the central part of the molecule is essentially charge-free. This metallic state state for majority spins can be associated with the peak in the conductance seen in Fig. (4.3) slightly below E_F. In the case of higher energies, the minority spins become conducting. In fact, the charge density for minority spins in the $[0.0, 0.5]$ eV energy interval (see fig. (4.7Bb)) is strikingly similar to the one presented in fig. (4.7Aa), which leads us to conclude they correspond to the same molecular state with a spin polarisation induced by the leads.

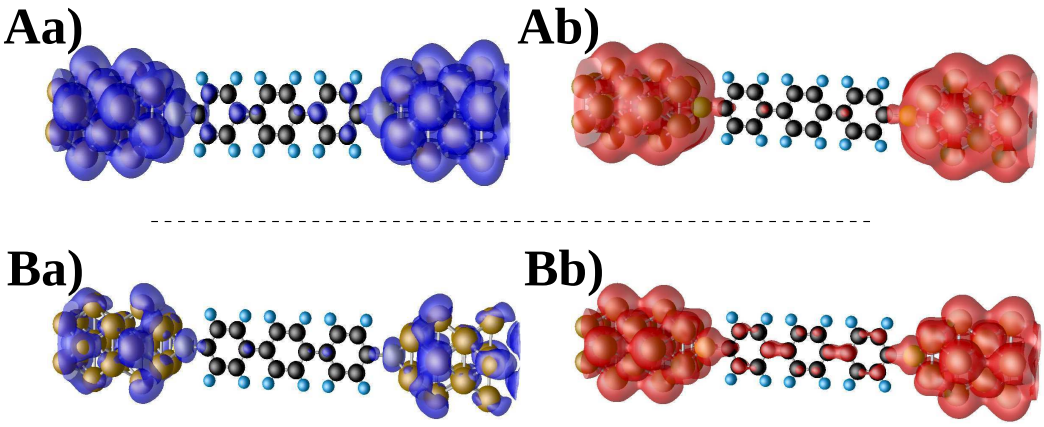

Figure 4.7: Local charge density Δn, for 1,4-triphenyl-dithiolate attached to nickel leads in the parallel alignment of the electrodes. The top panels are for the (A) -0.5 to 0.0 eV energy interval and bottom part for (B) 0.0 to 0.5 eV: (a) majority (blue iso-surface) and (b) minority (red iso-surface) spins. The iso-surfaces were taken for $\Delta n = 0.004\ |e|/Bohr^3$.

Turning our attention to the anti-parallel case we can understand the reasons for the smaller conductance seen in fig. (4.3c). On the right hand-side lead, majority electrons turn into minority and *vice-versa*. Hence, we can think of the states in Fig. (4.8) as being formed by exchanging the majority (minority) spins from the left hand-side with the minority (majority) spins from the right hand-side. If we divide our system in two parts, we can clearly see that the left hand-side of the molecules in Fig. (4.8) are identical to the ones in Fig. (4.7) whereas a and b are interchanged for the right hand-side.

In essence the molecule can be split into two disjoint sides. The total transmission is determined by the interplay between the energy-dependent transmission probabilities for each side separately as presented in figure (4.6). In the PA configuration it leads to high (low) conductance for the majority (minority) at E_F while it results in a convolution in the AA alignment.

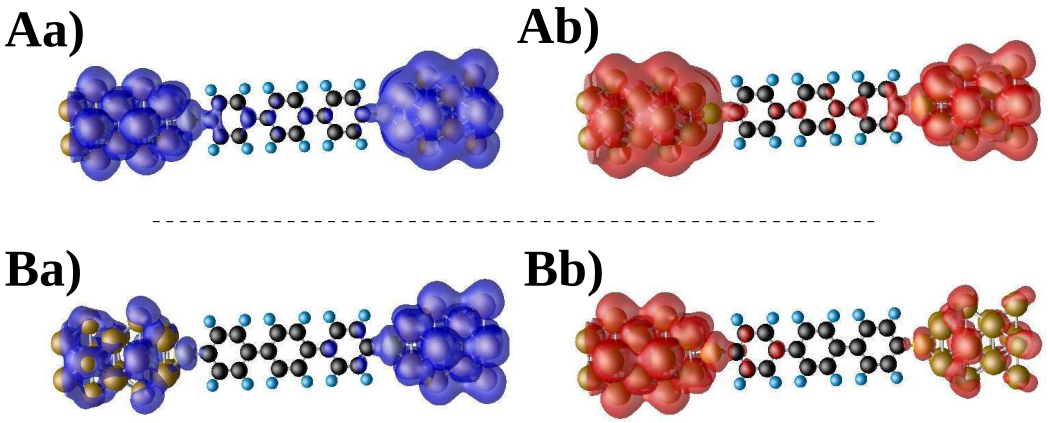

Figure 4.8: Local charge density, Δn for 1,4-triphenyl-dithiolate attached to nickel leads in the anti-parallel alignment of the electrodes. The top panels are for the (A) -0.5 to 0.0 eV energy interval and bottom part for (B) 0.0 to 0.5 eV: (a) majority (blue iso-surface) and (b) minority (red iso-surface) spins. The iso-surfaces were taken for $\Delta n = 0.004\ |e|/Bohr^3$.

An extreme - and idealised - case is when only one spin couples to the molecular state. Then the total transmission in the antiparallel case is identically zero since either $t^{\uparrow}$ or $t^{\downarrow}$ vanishes. This is the most desirable situation in real devices since, in principle, an infinite R_{GMR} can be obtained. Note that in this situation the system leads+molecule behaves as a half-metal although the two materials forming the device are not half-metals themselves. An even more extreme situation is when for a particular energy window the transport is through two distinct molecular states, which are respectively coupled to the majority and minority spin only. This may happen for instance due a particular symmetry of the molecular anchoring groups. Then in this energy window (see figure 4.9)

$$T^{\uparrow\uparrow}(E) \neq 0 \quad , \quad T^{\downarrow\downarrow}(E) \neq 0 \tag{4.7}$$

$$T^{\mathrm{PA}}_{\mathrm{Total}} = T^{\uparrow\uparrow} + T^{\downarrow\downarrow} \neq 0 \tag{4.8}$$

but

$$T^{\mathrm{PA}}_{\mathrm{Total}} = 2T^{\uparrow\downarrow} = 2t^{\uparrow}t^{\downarrow} = 0. \tag{4.9}$$

One possible way to achieve this situation (of infinite GMR) is to change the functional group that links the molecule to the surface, leading to different bonding properties specially in materials with highly directional coupling. Transition metals where d orbitals play an important *role* are likely candidates as opposed to noble metals where the chemical bonding is dominated by s orbitals with no angular

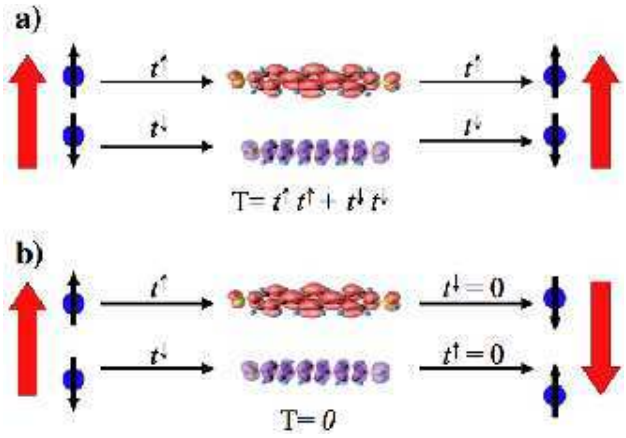

Figure 4.9: Scheme of the spin-transport mechanism through two energetically closely spaced molecular states. The first state (red) couples only to the majority spin band, while the minority spin couple only to the purple state. In the parallel case one finds $T^{\uparrow\uparrow}(E) \neq 0$ and $T^{\downarrow\downarrow}(E) \neq 0$ but in the antiparallel $T^{\uparrow\downarrow}(E) = 0$. We then expect an infinite GMR for such an energy window.

dependence [178]. The other possibility is to change the electrode itself. This is somewhat more complicated, but one can use an STM tip positioned at different lateral positions to probe different coupling configurations between the molecule and the tip itself. We will address these possibilities further on in this chapter.

4.3 Octane-dithiolate: tunnelling regime

The other family of molecules we have considered is the alkane family. Alkanes are single bond CH_2 groups that form a zigzag structure. Figure (4.10a) shows one such alkane with eight carbon atoms (octane) terminated with sulphur groups at both ends and connected to nickel electrodes in a similar fashion to the tricene molecule. These molecules have been recently used in pioneering molecular spin valve experiments by Petta *et al.* [49] although a theoretical description is still lacking.

As a starting point we performed DFT atomic relaxations on this molecule attached to nickel leads in the same way described in the previous section. The first difference from the tricene molecule presented in the previous section is the arrangement on surface; the preferred configuration of octanes on a [001] Ni surface is at an angle of approximately 36° from the normal to the surface.

The two molecules also present rather different electronic properties. Figure (4.10b) shows the density of states and local charge density for octane-dithiol. The HOMO-LUMO gap is now approximately 5 eV, almost double than that of tricene-

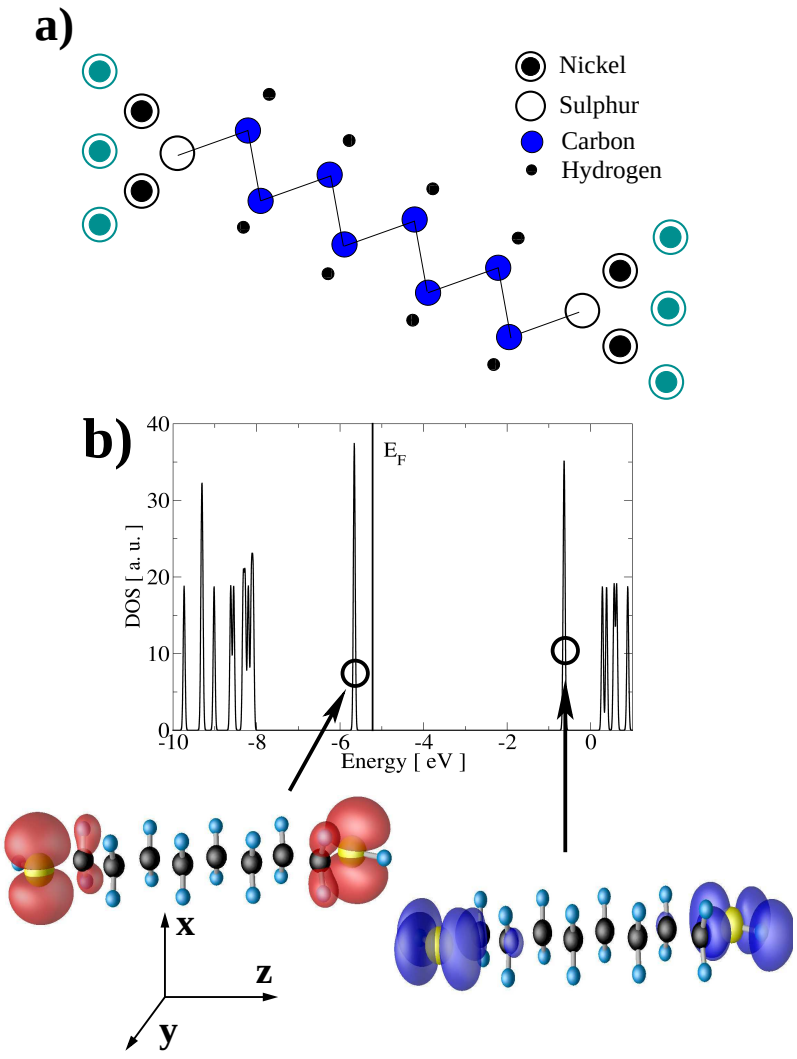

Figure 4.10: Structural and electronic properties of a Ni[001]/octane/Ni[001] spin-valve. a) Schematic structure of the octane molecule attached to [001] Ni surfaces. b) Density of states and charge-density iso-surface plots for the relevant molecular states of the isolated octane-dithiol molecule. The highest (lowest) "circled" state is the LUMO (HOMO) for such an isolated molecule. Because isolated levels correspond to delta functions in the DOS, for display purposes and to aid comparison with Fig. (4.11) we have artificially broadened the DOS by 0.1 eV.

dithiolate. The local charge density shown in the same figure also present considerably different behaviour. For the previous molecule the charge density was delocalised over the entire backbone whereas in octane the charge is concentrated mostly on the two sulphur atoms at either end of the molecule. The HOMO and LUMO also have significantly different orbital characters. While tricene could be understood in term

of bonding and anti-bonding states of the same π orbitals, for octane the HOMO is dominated mostly by the S $3p_x$ (and some contribution from the outermost C atoms) and the LUMO is a combination of sulphur p_z and p_y atomic orbitals.

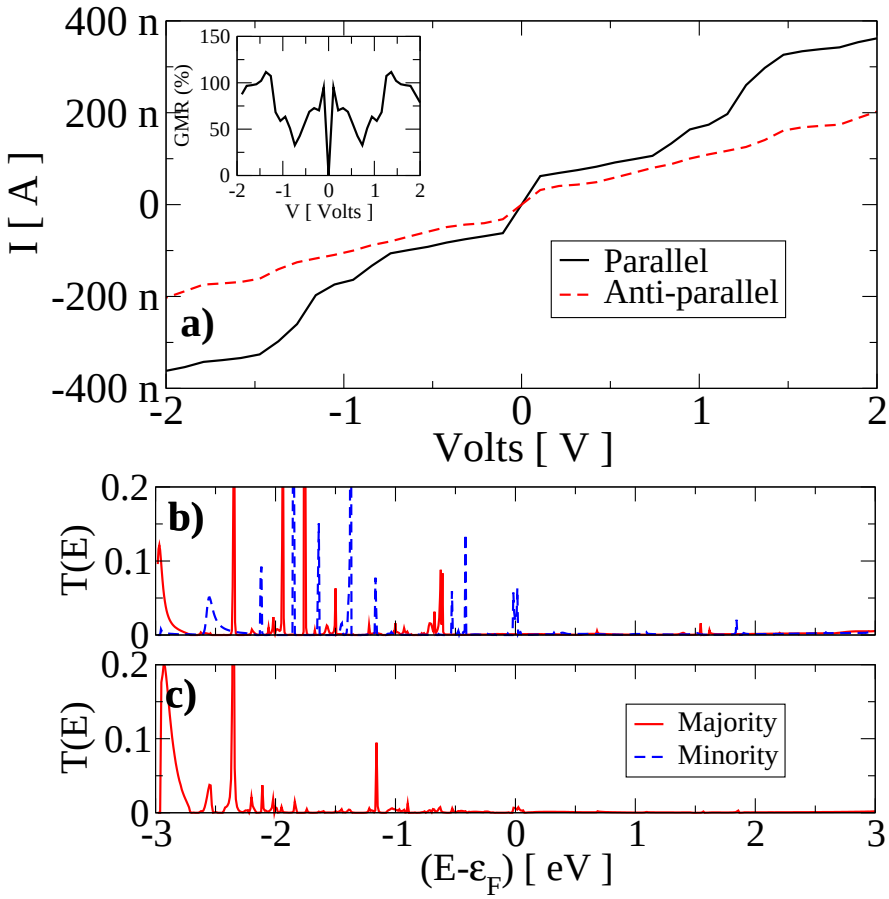

Figure 4.11: a) I-V characteristics for octane-dithiolate. b) Transmission coefficients at zero bias for majority (solid) and minority (dashed) spins. The inset shows the magnetoresistance as a function of bias.

The transport properties of octane-dithiolate are presented in Fig (4.11). At a more detailed level, it is clear that the two molecules possess rather different transport characteristics as well. In the case of octane the resistance is of the order of 10 MΩ with a current of about 150 nA at 1 V. This is in the same range as in recent experiments [49], although a direct comparison is difficult because the precise number of molecules bridging the two electrodes is unknown. However, the good agreement in terms of resistance gives us confidence in the ability of our method to describe these devices. The largest contribution to the current comes from a sharp resonance of the transmission coefficient at the Fermi level (see Fig. (4.11b)). This is mainly

given by minority electrons and it is strongly suppressed in the antiparallel case. Because in the antiparallel configuration the transmission coefficients are essentially zero at any energy around the Fermi energy E_F, we can conclude that the suppression of the aforementioned peak is the main reason for the magnetoresistance.

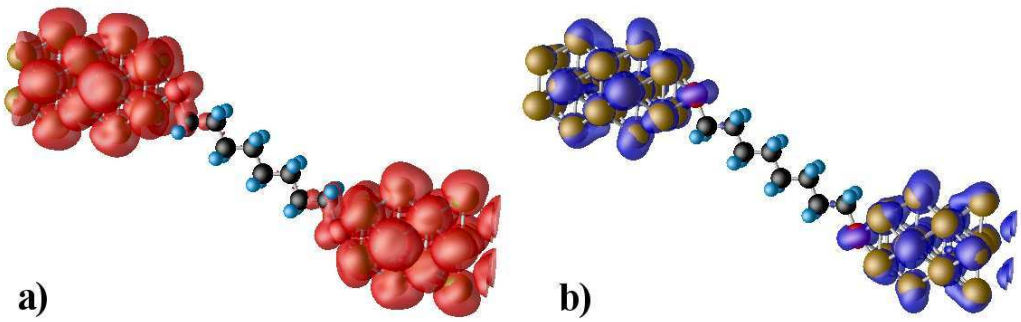

Figure 4.12: Local charge density Δn in the [E_F-0.25,E_F+0.25] eV region around the Fermi level for a) minority and b) majority spins in octane-dithiolate attached to a Ni [001] surface. We can clearly see that the minority spin spins dominate the Fermi energy and the backbone is devoid of charge. The iso-surfaces are cut at Δn=0.00015 $|e|/Bohr^3$.

A closer look at the orbital-resolved density of states of the conduction peak at E_F reveals that this is mainly due to Ni $3d$ and S $3p$ orbitals. The local charge density iso-surface plots which are shown in figure (4.12) also unambiguously prove that the charge density close to E_F is concentrated around the sulphur atoms and little density spreads over the carbon molecular backbone. The plots appear similar to those corresponding to the octane HOMO and LUMO states of Fig. (4.11b). This suggests that the transport is tunnelling-like through a Ni-$3d$/S-$3p$ surface state.

To further sustain this hypothesis we have calculated the transmission coefficients $T(E)$ at zero bias for various n-alkane molecules as a function of the number of carbon atoms n (n = 4, 6, 8 and 10). This reveals an exponential decay

$$T \propto e^{-\beta n} \tag{4.10}$$

with exponent $\beta = 0.88$, which clearly demonstrates that we are in a tunnelling regime. It is interesting to note that such an exponent is similar to the one found for the same molecule attached to gold [111] surfaces [207]. In addition we observe that the S atoms anchoring the octane molecule present an induced magnetic moment of $\sim 0.07\mu_B$ oriented in the same direction as the nickel magnetisation. The presence of charge density at the sulphur atoms is also a feature found for 8-alkane-dithiolate

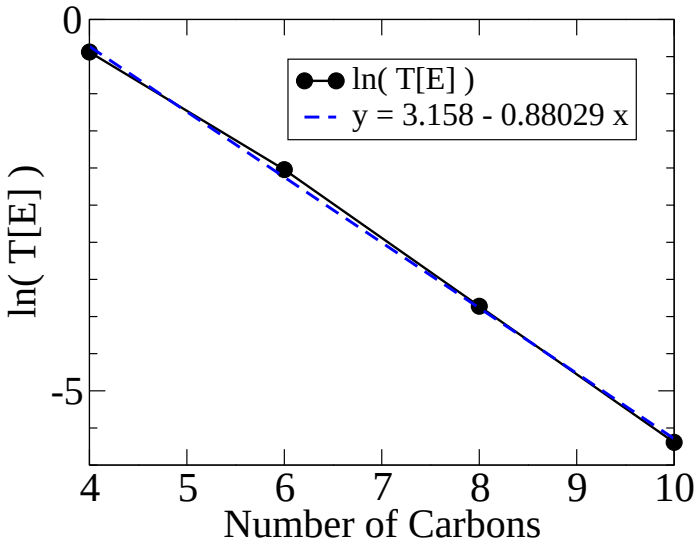

Figure 4.13: Distance dependence of the zero-bias transmission coefficients of octane-dithiolate; calculations (solid + filled circles) and linear regression (dashed).

on [111] gold surfaces, and it is related to the fact that the Fermi level lies in the molecular HOMO-LUMO gap [207].

The GMR in this case is significantly smaller than tricene, between 40% and 100%. This result is slightly larger than experimental results obtained for actual devices [49], however one expects that the geometry of the leads, orientation of the magnetisation and short circuiting through pin-holes might account for the discrepancy.

4.4 1,4-benzene-(S, Se, Te): end-group engineering

In the previous two sections we have shown how two different molecules can give different magneto-transport properties and GMR. Following the idea of appropriately selecting the molecule to enhance the magnetoresistance, one interesting aspect that calls our attention is the possibility to tailor the GMR according to the anchor group (AG).

We have explored this avenue [71, 88] by replacing the standard thiol group on phenyl-type molecules with either a Se or a Te atom. We considered the shorter 1,4-benzene molecules. As we can see from figure (4.4) the qualitative transport properties remain essentially unchanged independent of the number of phenyl rings even though the actual values of the transmission coefficients are different. This

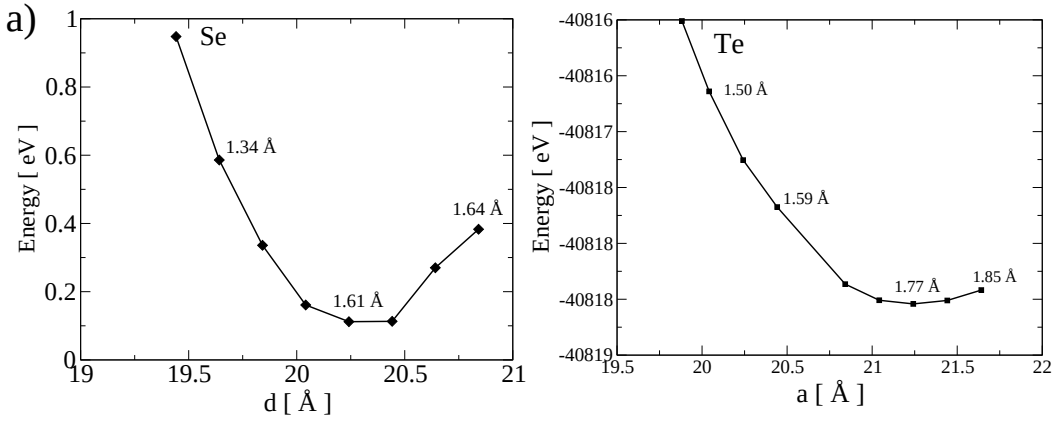

Figure 4.14: Total energy curve as a function super-cell size in a) 1,4-benzene-Selenium and b) 1,4-benzene-Tellurium.

result justifies our analyses of benzene-type molecules as a whole.

We considered three different anchoring groups, namely: sulphur (the standard AG in molecular electronics), Selenium and Tellurium. It is no coincidence that these three atoms belong to the same family of the periodic table. One would expect they have similar chemical and bonding properties, but different atomic radius.

In order to study the effects of different end-groups we first performed atomic relaxations to determine the arrangement of these new molecules on the magnetic surface. The initial configuration was similar to the one presented in figure (4.1) upon substitution of the sulphur atom - represented by the red sphere - by either Selenium or Tellurium. The CG relaxations were performed keeping the two outermost layers on either side of the super-cell fixed. The remaining central region was allowed to relax . We then vary the length of the cell d to minimise the total energy of the system. This method was applied in similar fashion as in chapter 3.

The selenium and tellurium atoms were modelled using respectively $3d^{10}4s^24p^4$ and $4d^{10}5s^25p^4$ as the initial atomic configurations. In both cases we used a DZ basis set for s and d and DZP for the p orbitals to account for the bonding properties.

The total energy curves for 1,4-benzene-selenium and -tellurium as a function of the total super-cell length are shown in figure (4.14). In the case of Tellurium the distance between the AG and the Ni surface is approximately 1.77 Å compared to 1.61 Å for Selenium and 1.26 Å for sulphur. Theoretical predictions of the transport properties of phenyl-tellurium and -selenium molecules attached to gold electrodes have been considered previously [208]. However the authors did not take into account the atomic relaxations due to changes in AG and the significant changes in the distance to the electrodes.

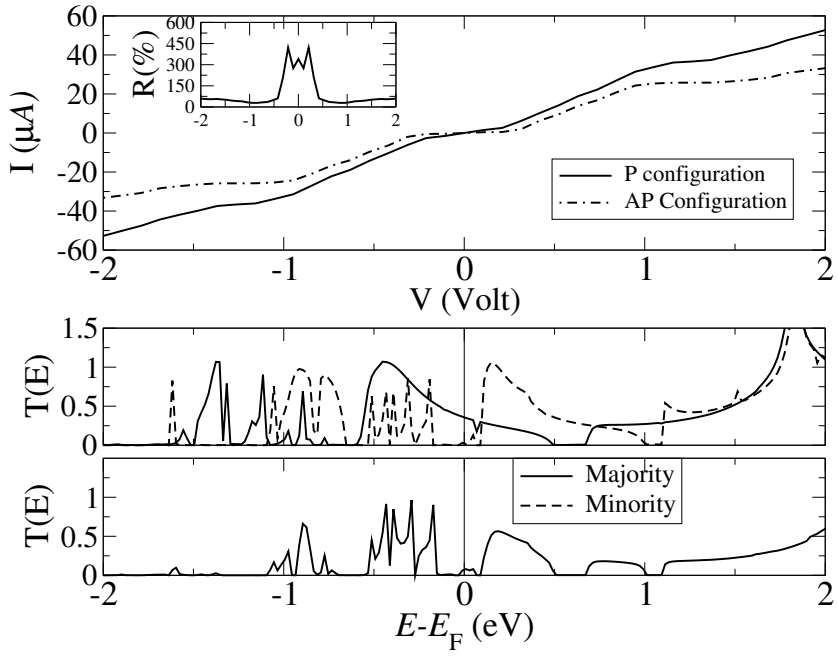

Figure 4.15: Transport properties for a 1,4-phenyl molecule attached to Ni (100) surfaces through a S group. The top panel shows the *I-V* characteristics for both the parallel and antiparallel alignment of the leads and the inset the corresponding GMR ratio. The lower panel is the transmission coefficient at zero bias as a function of energy. Because of spin-symmetry, in the antiparallel case we plot only the majority spin.

The transport properties of the three different molecules are presented in figures (4.9), (4.15) and (4.16). We can clearly see that the current as well as the transmission decreases as we go from sulphur down to selenium and then tellurium. As the molecules become more loosely coupled, the GMR increases reaching in excess of 450 % (figures' insets).

Albeit the higher GMR ratios the main transport properties are remarkably similar. In the PA alignment the HOMO is spin-split with the majority spin below and the minority spin above the Fermi level. We observe an overall reduction of the transmission coefficients for both majority and minority spins. However, for majority spins, given the strong hybridisation, the quenching of the transmission coefficients is not as significant as for the minority spins. Transmission probabilities for minority spins close to E_F are mostly due to tunnelling through Ni *d* states which are fairly localised. When we consider the AA configuration the convolution between majority and minority spins leads to much lower conduction because minority spins set the

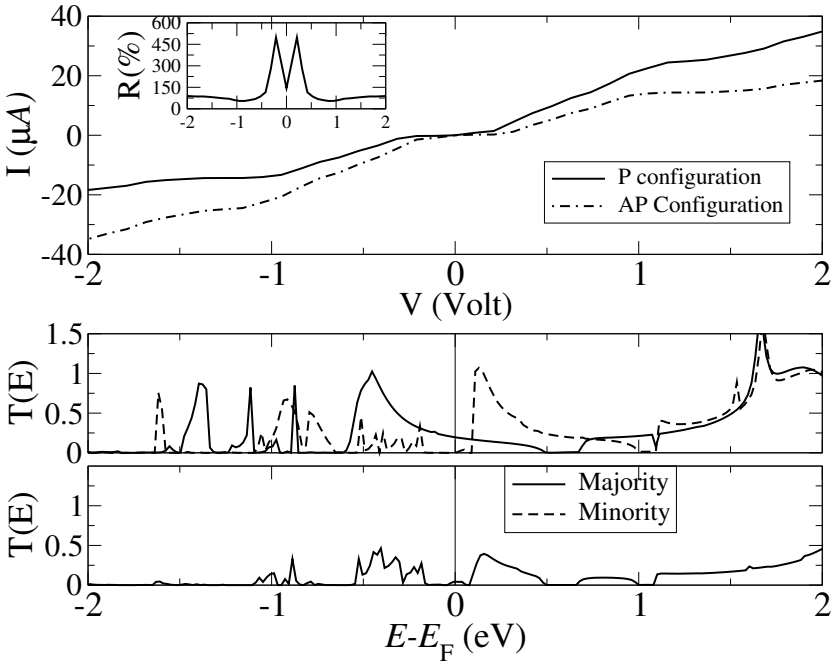

Figure 4.16: Transport properties for a 1,4-phenyl molecule attached to Ni [001] surfaces through a Se group. The top panel shows the I-V characteristics for both the parallel and antiparallel alignment of the leads and the inset the corresponding GMR ratio. The lower panel is the transmission coefficient at zero bias as a function of energy. Because of spin-symmetry, in the antiparallel case we plot only the majority spin.

bottleneck.

Essentially, the overall increase in the R_{GMR} is mainly due to an increase in the radius of the AG. Conduction through minority states which is mostly d-dominated is reduced more drastically than majority spin states.

4.5 Asymmetric molecules

In section (1.7) we used a simple one-energy-level model to show that charging effects on molecular states combined with asymmetric coupling to the electrodes can lead to asymmetries in the $I - V$ characteristics. This effect can be combined with a more realistic transport theory to design molecular devices which present highly asymmetrical characteristic curves. Ideally one can envisage a molecular substitute to standard solid-state diodes where current flows for forward bias, but is completely blocked for negative ones (or *vice versa*). In the case of spin-transport we can obtain

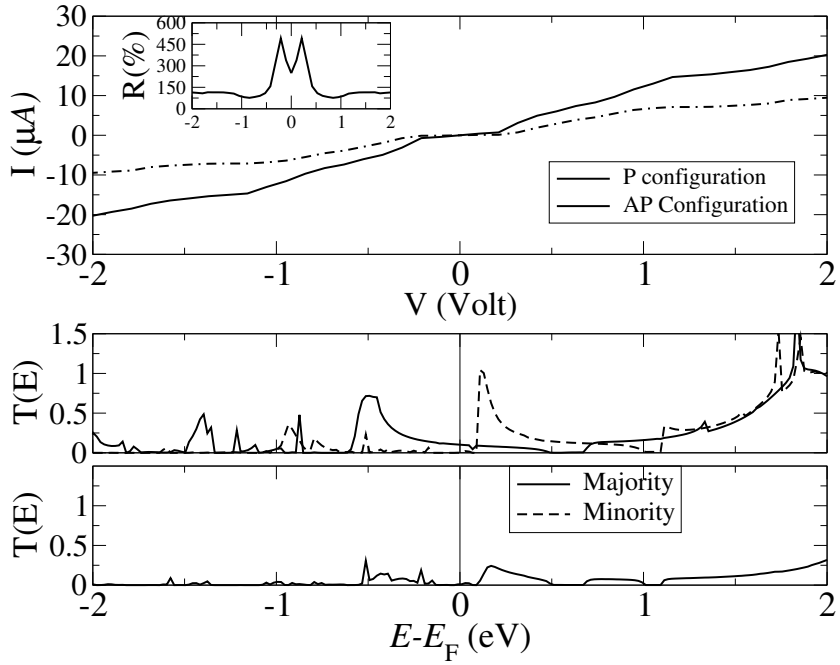

Figure 4.17: Transport properties for a 1,4-phenyl molecule attached to Ni [001] surfaces through a Te group. The top panel shows the I-V characteristics for both the parallel and antiparallel alignment of the leads and the inset the corresponding GMR ratio. The lower panel is the transmission coefficient at zero bias as a function of energy. Because of spin-symmetry, in the antiparallel case we plot only the majority spin.

devices for which one spin channel is completely blocked for forward bias, but not for negative voltages thus making a spin diode. We can then take the idea of end-group engineering one step further by using different AGs for either side.

The molecule we used is 1,4-benzene-tellurium-thiolate. It consists of a benzene ring terminated by a sulphur and a tellurium atom. The molecule is attached via sulphur and tellurium to two Ni [001] surfaces. Here we used periodic boundary conditions along the transverse direction with a 3x3 k-point mesh. A sketch of our system is shown in figure (4.18). The introduction of periodic boundary conditions in the transverse direction provides the correct description of the surface, more importantly we avoid mini-gaps in the band structure of the electrodes which can lead to spurious results. A possible drawback of this approach is that we are in fact modelling a monolayer of organic molecules between two Ni surfaces. In order to suppress inter-molecular interaction we make the lateral size of the super-cell rather big.

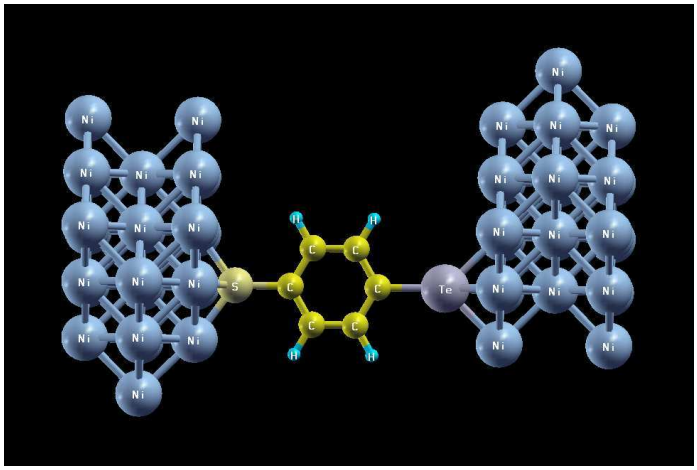

Figure 4.18: Ball-and-stick representation of a 1,4-benzene-tellurium-thiolate molecule attached to Ni [001] surfaces through the hollow site. The sulphur and tellurium atoms are attached to positions 1 and 4 respectively.

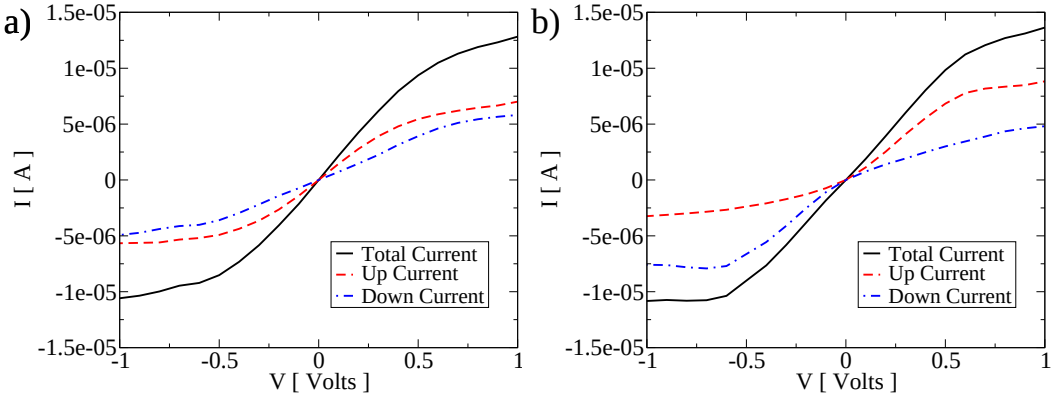

Figure 4.19: $I-V$ characteristics of 1,4-benzene-tellurium-thiolate molecule sandwiched between two Ni [001] surfaces.a) Parallel and b) anti-parallel configurations.

In figure (4.19) we analyse the $I-V$ characteristics our device. As we can see both the PA and AA configurations are reasonably asymmetric (the current for forward bias is only 20-25 % higher). Besides, the polarisation, P (defined in equation (3) for the antiparallel case is also significant reaching approximately -50 % at -0.5 V (in the case of backward bias the minority spin current is larger in absolute terms then majority spin one).

The GMR ratio for this molecule is presented in Fig. (4.20) and it also shows some interesting features. The spin-resolved magnetoresistance ratios are calculated

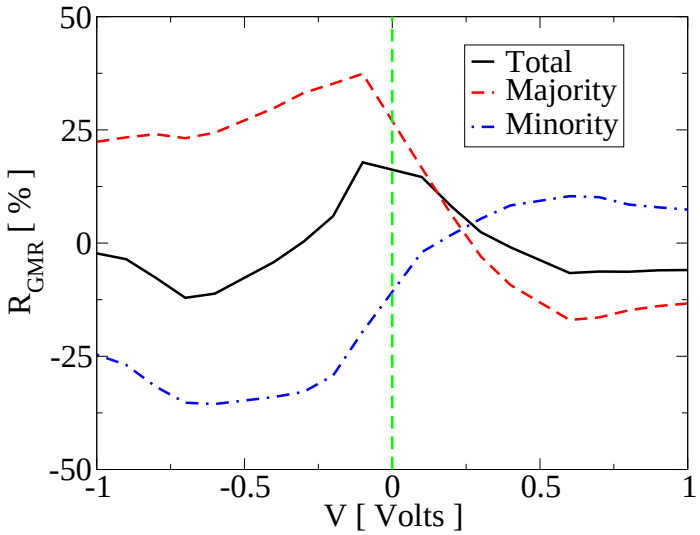

Figure 4.20: Giant-magnetoresistance ratio as a function of applied bias for BDTT molecule. The spin resolved GMR is calculated according to equations (4.11) and (4.12).

using

$$R^{\uparrow}_{\mathrm{GMR}} = \frac{I^{\uparrow}_{\mathrm{PA}} - I^{\uparrow}_{\mathrm{AA}}}{I^{\uparrow}_{\mathrm{AA}} + I^{\downarrow}_{\mathrm{AA}}}, \tag{4.11}$$

$$R^{\downarrow}_{\mathrm{GMR}} = \frac{I^{\downarrow}_{\mathrm{PA}} - I^{\downarrow}_{\mathrm{AA}}}{I^{\uparrow}_{\mathrm{AA}} + I^{\downarrow}_{\mathrm{AA}}}, \tag{4.12}$$

so that

$$R^{\mathrm{Total}}_{\mathrm{GMR}} = R^{\uparrow}_{\mathrm{GMR}} + R^{\downarrow}_{\mathrm{GMR}}. \tag{4.13}$$

The total GMR oscillates between positive and negative values depending on the applied bias, but it does not exceed 20 %. The individual spin components of the GMR can in fact exceed that value. We can clear see from figure (4.20) that $R^{\uparrow}_{\mathrm{GMR}}$ and $R^{\downarrow}_{\mathrm{GMR}}$ have opposite signs for the entire bias range considered here. For forward bias the minority spins dominate the transport whereas for backward bias the majority sets the final sign of the total GMR. Therefore we can conclude that the total GMR is a balancing act between the two spin components.

Finally figure (4.21) shows the zero-bias transmission coefficients as a function of energy. We can see that the molecule is conducting both for the PA and AA alignments of the electrodes. This metallic behaviour prevents the molecule from charging once bias is applied. In that case the asymmetries are not as large as one might wish.

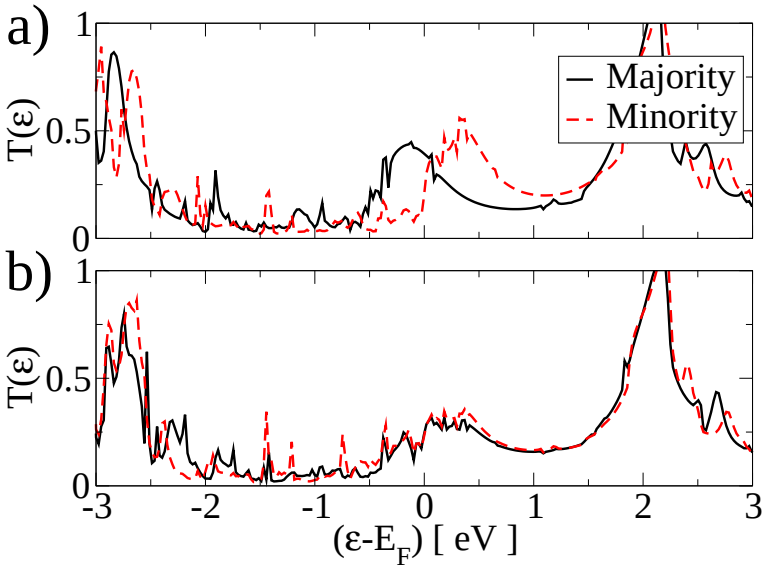

Figure 4.21: Transmission coefficients as a function of energy for 1,4-benzene-tellurium-thiolate sandwiched between Ni [001] surfaces: a) parallel and b) anti-parallel configurations.

4.6 Modelling scanning tunnelling microscopy with *Smeagol*

Instead of changing the anchoring groups as we did in the previous section it is also possible to tune the transport properties of organic molecules by attaching them to different sites [209]. In gold and other noble metals the bonds have mostly s character and have no angular dependence. In transition metals, on the other hand, d orbitals play an important role and the coupling of the molecule to different orbitals might lead to significant changes in the transport properties of a molecular device

The perfect tool for probing these properties is a STM [1]. In an STM one uses a metallic tip to measure the tunnelling current between a surface and the metallic tip itself. These tunnelling currents (usually ranging between nA and pA) can then be used to produce atomic resolution images of the surface and of molecules deposited on them [210]. The magnetic properties of surfaces can also be measured by using spin polarised STM [211, 212, 213]. Standard theory of STM's uses a convolution of the local density of states of the tip and the surface to describe the imaging process. In essence, the images produced are a fingerprint of the local density of states of the surface. It is usually assumed that tip and surface do not interact an approximation that has recently been called into question [214, 215].

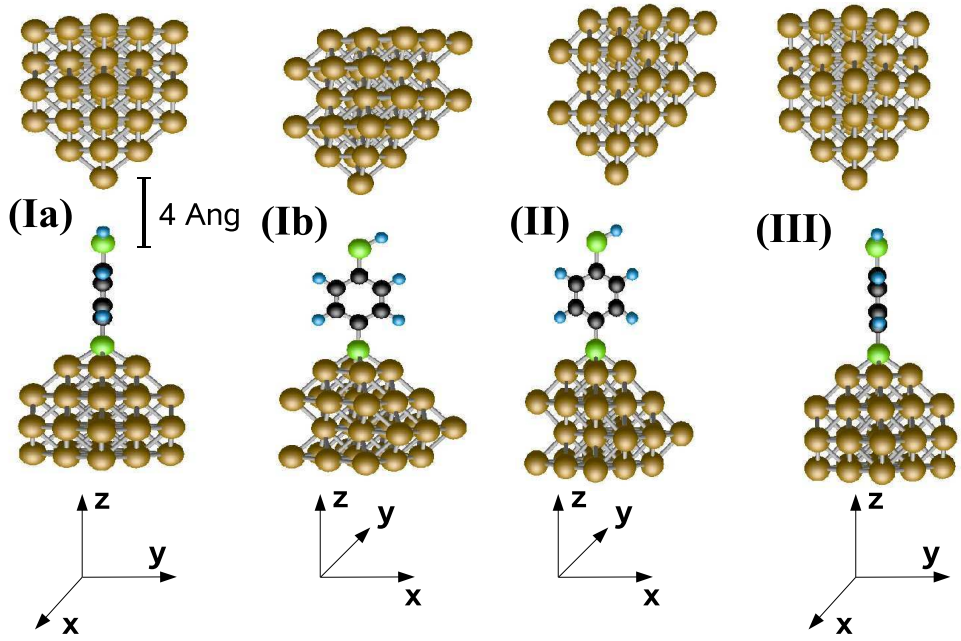

Figure 4.22: Ball-and-stick configurations of a 1,4-benzene-thiol-thiolate molecule in an STM setup. (Ia) side view; the tip is in the plane of the molecule on top of the sulphur atom, $\vec{r}_{\rm tip} = (0, 0, 4)$ Å. (Ib) top view for the same configuration as (Ia). (II) Side view; the tip is in the plane of the molecule on top of the hydrogen atom, $\vec{r}_{\rm tip} = (1.18, 0, 4)$ Å (III) side view; the tip is shifted upwards with respect to the molecular plane, $\vec{r}_{\rm tip} = (0, 1.18, 4)$ Å. In all cases we consider that positive bias is applied from the bottom - the surface. Legend: carbon - black, sulphur - green, hydrogen - light blue and nickel - brown.

More recently the STM has been used for measuring transport properties of nanoscale devices. Onishi and coworkers have used STM's to produce monoatomic metallic wires and to measure conductance quantisation [151].

In principle, an atomically sharp STM tip can be used to probe different orbitals of a single molecule. Hence, a theoretical description capable of describing the transport properties of STM in contact mode as well including tip/surface interactions in standard STM experiments is potentially useful in the field of nanoscience.

As a proof-of-concept we performed calculations on a benzene-dithiol molecule adsorbed on a nickel [001] surface. As the molecule approaches the surface the hydrogen atom bonded to the sulphur is removed, thus becoming a thiolate group, whereas the free standing thiol group at position 4 remains unchanged. The resulting

molecule is known as 1,4-benzene-dithiol-dithiolate (BDTT).

In order to model the magnetic STM tip we assumed a pyramid of Ni atoms along the [001] direction. The base of the pyramid consists of a nine-atom square cross section and the apex is represented by a single nickel atom. Our calculations correspond to three possible positions of the STM tip with respect to the BDTT molecule. The configurations are shown in figure (4.22) and are referred hereafter as I, II and III. The planar distance between the sulphur and the final atom on the tip was kept at 4 Å (see Fig. (4.22a)).[1] In other words, if we let $\vec{r}_{\text{tip}}$ be the position vector between the sulphur atom and the apex atom of the tip, then $\vec{r}_{\text{tip}} = (x, y, 4)$ Å for every configuration.

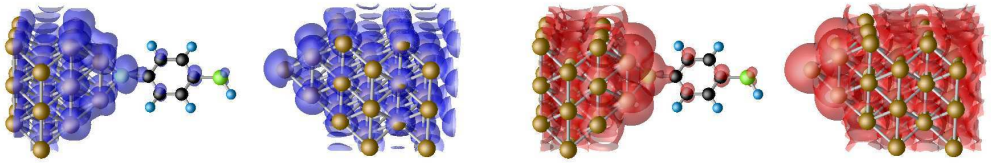

Figure 4.23: Local charge density of a 1,4-benzene-thiol-thiolate molecule attached a Nickel [001] surface probed by a Ni STM tip in configuration III. a) Majority and b) minority spins in the parallel configuration.

In configuration I (Fig. (4.22Ia-Ib)) the apex of the tip is positioned along the axis of the molecule, over the sulphur atom: $\vec{r}_{\text{tip}} = (0, 0, 4)$ Å. In arrangement II the tip shifts along the x axis to probe the H atom. In this case $\vec{r}_{\text{tip}} = (1.18, 0, 4)$ Å. Finally the tip is moved 1.18 Å away from the plane of the molecule, $\vec{r}_{\text{tip}} = (0, 1.18, 4)$ Å.

The calculations were performed with periodic boundary conditions in the lateral directions with a k-point sampling of 3×3 in the transverse Brillouin zone. The local charge density around E_F ([E_F-0.25,E_F+0.25] eV) for configuration III is shown in figure (4.23). We can see that the molecular orbitals on BDTT around this energy range are mostly carbon and sulphur π states. The local charge on the nickel surface and tip is higher in minority spin as expected. Changing the position of the tip does not significantly change the local charge density neither on the molecule nor on the tip.

In figure (4.24) we present the $I - V$ characteristics for all the tip configurations. We adopt the substrate as our reference electrode. In other words, positive bias means we shift the potential on the substrate upwards by $V/2$ and the potential on the tip downwards by $V/2$ (current from the substrate to the tip).

[1] We also performed calculations with distances of 2.5 Å and 3.0 Å with qualitatively similar

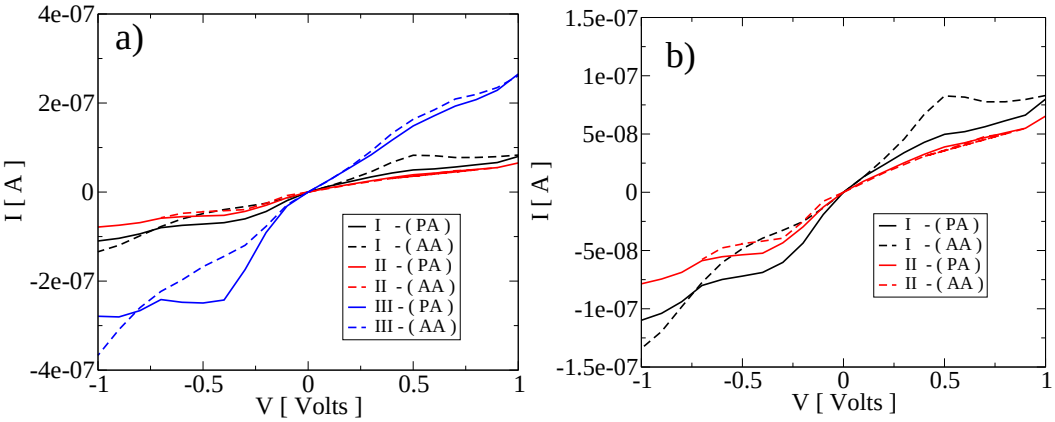

Figure 4.24: $I-V$ characteristics of BDTT attached to a Ni [001] surface through the hollow site and for different configurations of the STM tip. (a) arrangements I, II and III. (b) Focusing on arrangements I and II.

Although the absolute values of the $I-V$ characteristics are significantly different, we see a general trend in all curves, most notably the sign changes in the magnetoresistance ratios (when the current for the PA and AA configurations swap) occur at similar voltages. This is an indication that independently of the position of the tip, the states responsible for the transport properties are the same. Most notably in configurations I and II the transmission coefficients are very similar (see Fig. (4.25)). One notes that there is an overall reduction of the transmission coefficients, but the main features are the same.

The GMR ratio as a function of the applied bias is shown in figure (4.26). We can clearly see that the giant magnetoresistance ratio varies from approximately 80 to -50 % depending on bias and tip position.

The $I-V$ for configuration III deserves greater attention. Notably the current for this configuration is around twice as large as the other two arrangements, even though the distance between tip and molecule has effectively increased; $r^{\mathrm{III}}_{\mathrm{tip}} = r^{\mathrm{II}}_{\mathrm{tip}} > r^{\mathrm{I}}_{\mathrm{tip}}$.

This effect can be explained using the simple picture presented in figure (2). In essence the STM probes the π orbitals of the BDTT shown in Fig. (4.23). When the tip lies along the axis the coupling is smaller due to symmetry compared to the case where the tip is at an angle (above the plane of the molecule), consequently we see an enhancement of the conduction. The GMR for this device reaches approximately 60 %. Furthermore, it presents potential for rectification. Up to 0.4 Volts the current for negative voltages is approximately twice as large as the current for positive ones. On the other hand for higher negative bias the $I-V$ characteristics reaches a plateau

results.

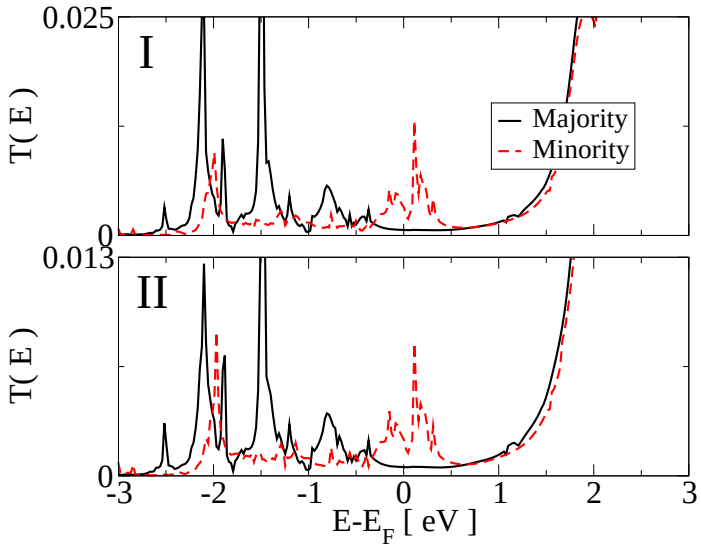

Figure 4.25: Transmission coefficients as a function of energy for the parallel configuration and different positions of the STM tip on the molecule. Note that the scales on the two graphs are different.

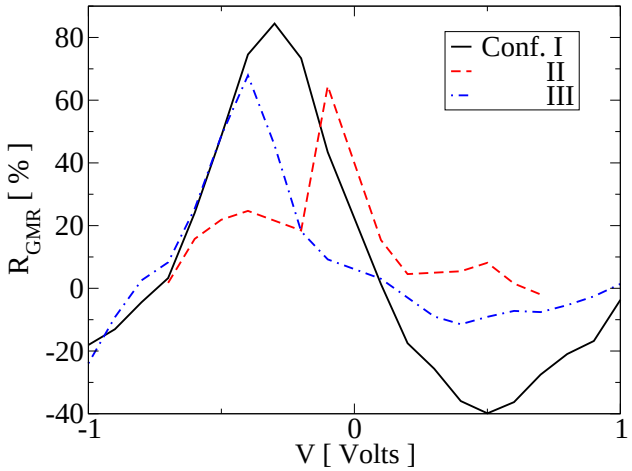

Figure 4.26: Giant magnetoresistance ratio as function of bias for different arrangements of the STM tip.

around and remains unchanged up to 1 Volt.

In order to analyse this curve we turn to the bias-dependent tranmission coefficients. For positive bias the results are shown in Fig. (4.27).

At zero bias we can clearly see two crests slightly below the Fermi level for majority spins and one above and another below the E_F for minority spins. The nature of these crests can be understood by looking at the projected of states of the entire system - Ni-surface/molecule/Ni-STM. We can see in figure (4.28) that there

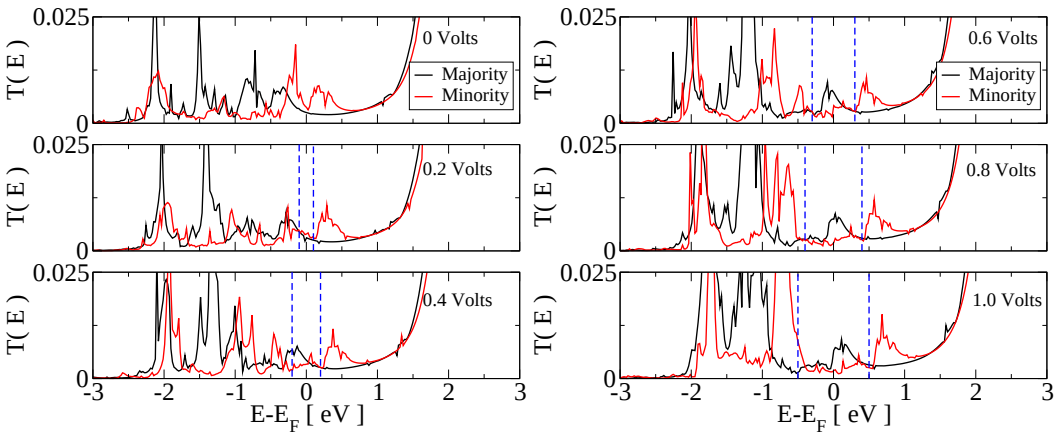

Figure 4.27: Transmission as a function of energy for BDTT attached to a Ni [001] surface for forward bias in configuration III.

are two states - for both majority and minority spins - which are close in energy to the zero-bias conductance peaks. The first state corresponds to a surface state on the nickel substrate which hybridises with the sulphur atom adsorbed on it. The second state is slightly lower in energy and is localised on the low-coordinated atoms of the tip. The existence of surface states usually lead sharp but high conductance peaks, but because the two contacts with the molecule present different electronic properties, these states lie at different energies in the PDOS: the system is off-resonance.[2]

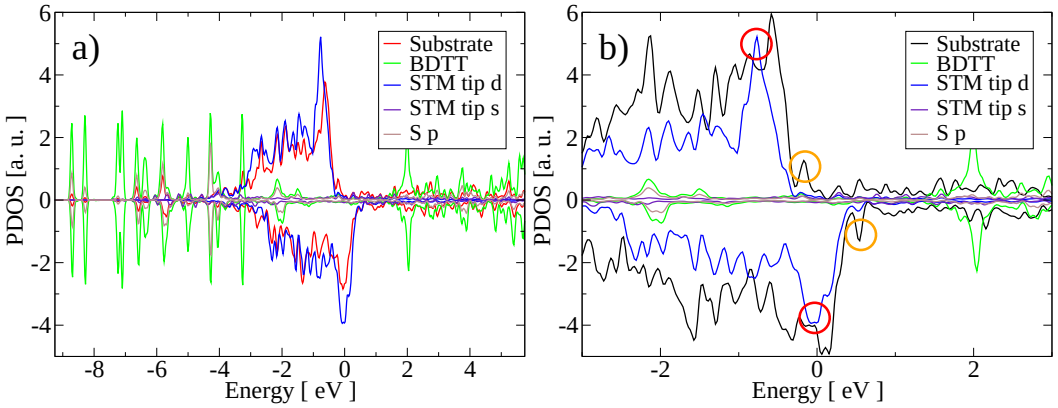

Figure 4.28: Projected density of states of the combined system surface/BDTT/tip. The states accounted for the transport in the surface and tip are circled in blue and red respectively. The bias window is indicated by vertical dashed blue lines.

[2]Resonant surface states have been observed in theoretical studies of point contacts [216] and tunnelling junctions [145] where both electrodes are similar. Usually impurities and the introduction of bias lead to a quenching of these states in experiments.

As we apply a positive bias the surface state, which is higher in energy (orange circle in Fig. (4.28)), moves upwards and the tip state moves downwards. This means they never overlap and the current monotonically increases as we open the bias window. When we apply a negative electric field the opposite occurs, we can see from figure (4.29) that these states move within range of each other at around -0.4 Volts creating a resonant state represented by a peak in the transmission coefficients. Most notably, for minority spins, this resonant state lies within the bias window thus leading to higher currents.

As we keep increasing the bias, the states come off resonance again. Although the integration range for the current increases the conductance peaks shrink which in turn results in the current *plateau* of figure (4.24a).

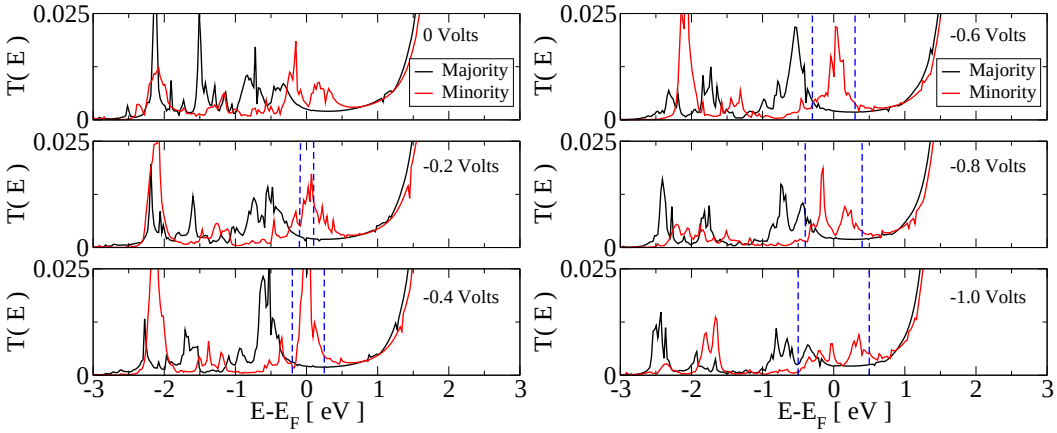

Figure 4.29: Transmission as a function of energy for BDTT attached to a Ni [001] surface for backward bias in configuration III. The bias window is indicated by vertical dashed blue lines.

This plateau will remain unchanged until we reach the LUMO of the molecule (around 1 eV above the Fermi level) whereas for forward bias the current keeps increasing monotonically. This leads to a swap in the rectification process. Hence, by appropriately selecting the voltage one can tune the rectification properties of the molecule.

In the AA alignment there is never a resonant state, nevertheless the degree of rectification is also large. At 1 Volt it is approximately 30 %.

Hence we have shown that by changing the position of the spin polarised STM tip with respect to an organic molecule we can obtain an enhancement of the current by probing different molecular orbitals as well as highly asymmetric $I-V$ characteristics. The correct description of the bias ramp results in interesting phenomena such as resonance states and current rectification.

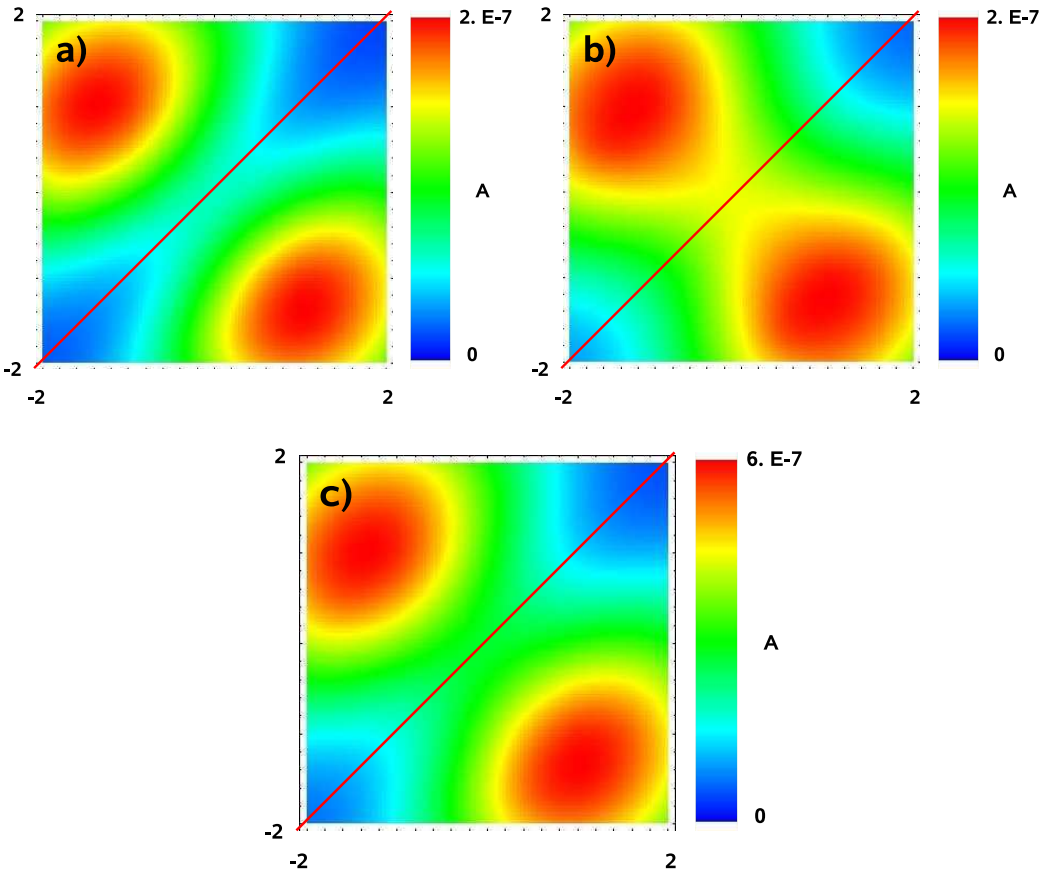

Figure 4.30: Theoretically calculated STM image of a benzene-thiol-thiolate molecule attached to a Ni surface probed by a Ni STM tip. a) Majority spin current, b) minority spin current and c) total current. The molecule lies along the diagonal depicted by the red line.

We can go one step further an calculate an STM image using the NEGF approach. By calculating the non-equilibrium steady current at different lateral positions of the tip (keeping the distance between the apex Ni atom and the sulphur at 4 Å) we can reproduce the image of an STM experiment including the interaction between sample and tip, an effect usually neglected in simulations of this type [215]. In figure (4.30) we show a surface plot resulting from calculating the current at an applied bias of 500 mV between sample and tip. We considered here only the AA configuration. The plane of the benzene molecule lies along the diagonal (the red line). Hence, we observe higher currents above and below the plane of the molecule. This is an indication that we are imaging the delocalised π orbitals of the benzene molecule. Most notably there is no signature of the hydrogen atom even though it lies closer

to the Ni tip.

4.7 Conclusion

In this chapter we have shown that molecules can give rise to large GMR when sandwiched between magnetic electrodes. We have shown that conducting molecules such as triphenyl-dithiol can show much larger GMR than insulating ones such as alkane-dithiol molecules. The GMR ratios can vary up to 650% in some cases.

We have also explored the possibility to engineer the end-groups to achieve optimal magnetoresistance. In that case we used other end-group atoms such as selenium and tellurium, belonging to the same family of sulphur in the periodic table. The increase in atomic number and atomic radius is the main cause in the increase in GMR. This shows how we can engineer the magnetoresistance by making an appropriate choice of molecule and end-group.

Finally we explored the idea of diode-like magnetic devices by using charging effects combined with asymmetric coupling to the electrodes. In the case of a phenyl-tellurium-thiolate molecule we obtain large polarisation of current, but relatively small rectification due to the metallic nature of the device.

In the case of STM-like devices the rectification can be much large and we also showed how change the $I - V$ characteristics by probing different states of the molecule.